

Article

Analytical Solution of the One-Dimensional Transport of Ionic Contaminants in Porous Media with Time-Varying Velocity

Xing Zeng ^{*}, Tong Gao, Linhui Xie and Zijian He

Hunan Provincial Key Laboratory of Geotechnical Engineering for Stability Control and Health Monitoring, Hunan University of Science and Technology, Xiangtan 411201, China

* Correspondence: xzeng@hnust.edu.cn

Abstract: The one-dimensional convection–dispersion equation has been widely used to describe the migration process of contaminant leachate through barriers. However, most of the existing solutions are limited to simple conditions. In this study, a one-dimensional convection–dispersion model with time-dependent velocity was established while considering the change in the permeability coefficient. The analytical solution of the model was obtained by using the integral transformation method. Based on the analytical model, three special conditions were assumed for comparison. The results showed that the concentration levels of pollutants inside the barrier would significantly increase with the increase in the flow velocity, and the pollutant concentrations inside the barrier would be increased by four times compared with the normal flow velocity when the flow rate increased by two times. The transports of heavy metal ions with variable velocities through soil–bentonite and soil–attapulgite barriers were predicted under field conditions. The predicted results showed that the breakthrough time would be reduced by as much as two times. In engineering practice, a barrier’s service performance can be improved by controlling the temperature of the seepage field and improving the chemical compatibility of the barrier materials.

Keywords: permeability coefficient; contaminant migration; variable velocity; integral transformation; analytical solution



Citation: Zeng, X.; Gao, T.; Xie, L.; He, Z. Analytical Solution of the One-Dimensional Transport of Ionic Contaminants in Porous Media with Time-Varying Velocity. *Water* **2023**, *15*, 1530. <https://doi.org/10.3390/w15081530>

Academic Editor: Constantinos V. Chrysikopoulos

Received: 9 March 2023

Revised: 5 April 2023

Accepted: 11 April 2023

Published: 13 April 2023



Copyright: © 2023 by the authors. Licensee MDPI, Basel, Switzerland. This article is an open access article distributed under the terms and conditions of the Creative Commons Attribution (CC BY) license (<https://creativecommons.org/licenses/by/4.0/>).

1. Introduction

Groundwater is a source of drinking water for many people around the world, so its quality is very important. With the continuous development of the world, contamination with the leachates of various human-made pollutants is becoming more and more serious [1–3]. These pollution sources mainly come from urban landfills and heavy metal mining areas, and they include organic chemicals, heavy metal pollutants, bacteria, and radioactive elements [4–6]. These substances easily migrate in groundwater [7–9]. One of the most important tasks in the environmental sciences consists of developing efficient and cost-effective techniques for remediating soil and groundwater contamination. In general, groundwater contamination is addressed through two different objectives: preventing the migration of contaminants from the source and, on the other hand, treating polluted aquifers by eliminating or at least reducing the concentrations of contaminants [10]. Underground horizontal and vertical engineered barriers are the main way to isolate pollutants in landfills and heavy metal mining areas. Therefore, it is particularly important to study the migration behavior of pollutants in engineered barriers [11–13]. The convection–dispersion model can describe the process of groundwater migration well. Relevant scholars at home and abroad have used the convection–dispersion equation to establish relevant models. Through its analytical and numerical solutions, the concentration levels of pollutants at different positions and times in the model can be described to illustrate the influences of pollutants [14–22].

The current research usually assumes that the permeability coefficient of the media will be constant for a period of time. The research of Liu Xia [23] and Zhang Jing [24] showed

that due to the large amount of heat energy generated in the process of waste degradation in landfills, the internal temperatures of landfills will rise. The internal temperatures of some special landfills can be as high as 80–90 °C. At the same time as the increase in temperature, the permeability coefficient of a barrier will gradually increase. This will lead to an increase in the migration rate of pollutants. Rao [25] believed that a reduction in the thickness of a double electric layer would make the micro-pores in bentonite develop into large pores, increase the flow space of the solution, and increase the permeability coefficient of bentonite. Zhu Wei [26] systematically studied the chemical compatibility of four vertical soil isolation barrier materials under the action of a calcium chloride solution. Malusis [27], Bohnhoff [28], and Xu [29] reported the chemical compatibility of a vertical sand–bentonite isolation barrier material under the action of a 0–1000 mmol/L calcium chloride solution and a simulated landfill leachate. As calcium ions and glucose in the solution compressed the double electric layers of bentonite particles, the permeability coefficient significantly increased, which led to an increase in the rate of contaminant migration.

All the above studies indicated that the permeability coefficient of porous media will change and the performance of barriers will deteriorate. If the permeability coefficient before deterioration is used for calculation, the predicted result is relatively conservative compared with that in the actual situation; if the permeability coefficient after deterioration is used for calculation, the predicted result is relatively exaggerated compared with that in the actual situation. Therefore, the long-term performance of a barrier can be more accurately predicted by considering the changes in the permeability coefficient in the model. Pickens [30] studied several forms in which the hydrodynamic dispersion coefficient changed over time by establishing a finite element model and obtained numerical solutions. Singh, M. K. [31] established a two-dimensional convection–dispersion governing equation without adsorption while considering the sinusoidal variation in flow velocity and obtained the analytical solution of two-dimensional convection–dispersion by using the Laplace transform method. Barry and Sposito [32] provided closed solutions for solute transport in a semi-infinite domain with time-varying dispersion coefficients, and arbitrary initial and boundary flux conditions were obtained through the separation of variables method. A simple numerical solution was also calculated and compared with the analytical solution, which was unstable for large values of Δt . Zamani and Bombardell [33] explored the analytical solution of the convection–dispersion–adsorption (ADR) equation, from which the variation in the pollutant percolation field could be found. Guerrero and Skaggs [34] used the generalized integral transformation technique (GITT) to analyze the analytical solution of the convection–dispersion equation for the variation in the dispersion coefficient with distance. Basha and El-Habel [35] presented an analytical solution for the linear and exponential variations in the dispersion coefficient over time in an infinite domain. Singh [36] proposed a one-dimensional analytical solution for the variations in dispersion coefficients over time in a homogeneous, semi-infinite porous formation. Yates [37] developed a one-dimensional non-homogeneous porous medium model for the spatial variations in the diffusion coefficients of pollutants. The model used a new variable transformation method to transform the problem of transport in non-homogeneous media into a problem of transport in homogeneous media, and it was able to accurately calculate the flow rates in different media. The accuracy of the model was verified with experimental data, and the applicability of the model in different non-homogeneous media was demonstrated. Atul [38] studied the analytical solution of a one-dimensional convection–dispersion equation with variable coefficients (the dispersion coefficient was proportional to the square of the velocity) in a semi-infinite medium. The main objective was to solve this equation with new mathematical methods that could be used to predict the transport of contaminants in groundwater.

The above literature review revealed that there are few contaminant transport models that take changes in permeability coefficients over time into account. In this study, we only address the special case of linearly increasing permeability coefficients of soil barrier materials (e.g., bentonite and attapulgite), establish a one-dimensional convection–

dispersion–adsorption equation, and use integral transformations to derive analytical solutions for the case of changing pollutant flow rates so that the study of groundwater pollution migration patterns can be more in line with practical needs.

2. Basic Assumptions and Calculation Model

2.1. Basic Assumptions

In this paper, the convection–dispersion model of pollutants in the soil is established based on the following assumptions: (1) The clay is homogeneous and saturated; (2) the diffusion of pollutants in soil follows Fick’s first and second laws; (3) the convection–dispersion equation involves one-dimensional transport; (4) the adsorption process is assumed to be linear and reversible; (5) the contaminant diffusion coefficient has a positive correlation with the percolation velocity and has a maximum value; (6) the model is semi-infinite and the contaminant transport is a variable-velocity flow that takes the change in the permeability coefficient into account.

2.2. Governing Equations and Solution Conditions

In general, the convection–dispersion equation with adsorption is expressed in one-dimensional Cartesian coordinates as

$$R \frac{\partial C}{\partial t} = \frac{\partial}{\partial t} \left(D_h \frac{\partial C}{\partial z} - uC \right) \quad (1)$$

where C [ML^{-3}] denotes the solute concentration at position z [L] at any moment t [T]; D_h [L^2T^{-1}] and u [LT^{-1}] denote the hydrodynamic dispersion coefficient and percolation velocity along the longitudinal direction (Z -axis), respectively. The retardation factor is denoted by R . It is calculated by using the following equation.

$$R = 1 + \frac{\rho K_p}{n} \quad (2)$$

where ρ is the medium density; K_p is the distribution coefficient; n is the porosity. K_p is the slope of the adsorption isotherm, and when the adsorption isotherm is linear, K_p is called the distribution coefficient K_d .

The assumption in this study is that the permeability coefficient increases linearly with time; thus, the following relationship between the permeability coefficient and time is introduced:

$$k_s(t) = k_0(1 + at) \quad (3)$$

$$u(t) = \frac{k_s(t) \times i}{n} \quad (4)$$

where a is defined as the coefficient of influence; $k_s(t)$ is a function of the permeability coefficient and time; k_0 is the initial value of the permeability coefficient; $u(t)$ is a function of the flow rate and time; i is the hydraulic gradient; n is the porosity. Since this study ignores the effect of molecular diffusion, the hydrodynamic dispersion coefficient D_h can be expressed as:

$$D_h(t) = \alpha u(t) \quad (5)$$

where $D_h(t)$ is a function of the hydrodynamic dispersion coefficient; α is the longitudinal dispersion. Based on the above theories and assumptions, a one-dimensional convection–dispersion model of contaminants in soil with a variable velocity is established. The governing equations of the problem can be described as follows:

$$\frac{\partial C(z, t)}{\partial t} = \frac{D_h(t)}{R} \frac{\partial^2 C(z, t)}{\partial z^2} - \frac{u(t)}{R} \frac{\partial C(z, t)}{\partial z} \quad (6)$$

Using Equations (3)–(5), the flow velocity and hydrodynamic dispersion coefficient can be expressed as

$$\begin{cases} V(at) = 1 + at \\ u(t) = u_0V(at) \\ D_h(t) = D_0V(at) \end{cases} \quad (7)$$

$V(at)$ is the linear relationship that is introduced; D_0 and u_0 are the initial values of $D_h(t)$ and $u(t)$, respectively; $D_0 = \alpha u_0$, $u_0 = u_a/n$, u_a is the Darcy flow rate, and $u_a = k_0i$. The assumed velocity of contaminant migration $u(t)$ is a piecewise function, and this piecewise function is as follows:

$$u(t) = \begin{cases} u_0(1 + at), & t_e > t \geq 0 \\ u_0(1 + at_e), & t \geq t_e \end{cases} \quad (8)$$

Suppose that at the start time, the model has the initial condition that the initial concentration of the pollutant in the medium is 0.

$$t = 0 : C(z, 0) = 0 \quad (9)$$

The initial concentration of the contaminant in the landfill is constant and is C_0 ; then, the boundary condition of the model is

$$z = 0 : C(z, t) = C_0 \quad (10)$$

The lower boundary conditions of the model are

$$z = \infty : C(z, t) = 0 \quad (11)$$

2.3. Solution of the Model

The original model governing Equation (6) can be changed to

$$\frac{\partial C(z, t)}{V(at)\partial t} = \frac{D_0}{R} \frac{\partial^2 C(z, t)}{\partial z^2} - \frac{u_0}{R} \frac{\partial C(z, t)}{\partial z} \quad (12)$$

The left side of the new governing Equation (9) is subjected to an integral transformation [39].

$$T^* = \int_0^t V(at)dt \quad (13)$$

The left side of the governing Equation (12) then becomes $\partial C/\partial(T^*)$, and T^* is a new time variable.

$$\frac{\partial C(z, T^*)}{\partial T^*} = \frac{D_0}{R} \frac{\partial^2 C(z, T^*)}{\partial z^2} - \frac{u_0}{R} \frac{\partial C(z, T^*)}{\partial z} \quad (14)$$

Then, the original initial and boundary conditions become

$$T^* = 0 : C(z, T^*) = 0 \quad (15)$$

$$z = 0 : C(z, T^*) = C_0 \quad (16)$$

$$z = \infty : C(z, T^*) = 0 \quad (17)$$

The model can be solved by using the integral transform. In the Laplace transform, when $t \geq 0$, $f(t)$ is defined. The integral is

$$F(p) = \int_0^t f(t) \exp(-pt)dt \quad (18)$$

The inverse transformation is, then,

$$f(t) = \frac{1}{2\pi i} \int_{\alpha-i\infty}^{\alpha+i\infty} F(p) \exp(-pt) dp \tag{19}$$

Multiplying both sides of the governing Equation (14) by $\exp(-pt)$ and integrating over t in the range $(0, \infty)$ results in

$$\int_0^\infty \exp(-pT^*) \frac{\partial C(z, T^*)}{\partial T^*} dT^* = \int_0^\infty \exp(-pT^*) \frac{D_0}{R} \frac{\partial^2 C(z, T^*)}{\partial z^2} dT^* - \int_0^\infty \exp(-pT^*) \frac{u_0}{R} \frac{\partial C(z, T^*)}{\partial z} dT^* \tag{20}$$

With the initial condition (9), $C(z, 0) = 0$, and by substituting (20), the result is

$$\begin{aligned} C(z, T^*) \exp(-pt) \Big|_0^\infty - \left[\int_0^\infty (-p) C(z, T^*) \exp(-pT^*) dT^* \times \int_0^\infty (-p) C(z, T^*) \exp(-pT^*) dT^* \right] = \\ \int_0^\infty \exp(-pT^*) \frac{D_0}{R} \frac{\partial^2 C(z, T^*)}{\partial z^2} dT^* - \int_0^\infty \exp(-pT^*) \frac{u_0}{R} \frac{\partial C(z, T^*)}{\partial z} dT^* = \\ \frac{D_0}{R} \frac{\partial^2}{\partial z^2} \int_0^\infty C(z, T^*) \exp(-pT^*) dT^* - \frac{u_0}{R} \frac{\partial}{\partial z} \int_0^\infty C(z, T^*) \exp(-pT^*) dT^* - C(z, 0) + p \int_0^\infty C(z, t) \exp(-pt) dt \end{aligned} \tag{21}$$

Then, the governing Equation (14) eventually takes the form

$$pC(z, p) = \frac{D_0}{R} \frac{\partial^2 C(z, p)}{\partial z^2} - \frac{u_0}{R} \frac{\partial C(z, p)}{\partial z} \tag{22}$$

Equation (22) is the changed governing equation, and the boundary conditions (16) and (17) are also transformed with the Laplace transform to obtain

$$z = 0 : C^*(0, p) = \frac{C_0}{p} \tag{23}$$

$$z = \infty : C(\infty, p) = 0 \tag{24}$$

The characteristic equation of (22) is obtained:

$$\frac{D_0}{R} r^2 - \frac{u_0}{R} r - p = 0 \tag{25}$$

Two eigenvalues can be obtained: $r_{1,2}$. The general solution is

$$C^*(z, p) = Ae^{r_1 z} + Be^{r_2 z} \tag{26}$$

$$r_{1,2} = \frac{u_0}{2D_0R} \pm \frac{1}{\sqrt{D_0R}} \sqrt{\frac{u_0^2}{4D_0R} + p} \tag{27}$$

The characteristic value $r_{1,2}$ is obtained substituting this into Equation (26):

$$C^*(z, p) = A \exp\left(\frac{zu_0}{2D_0R} + \frac{z}{\sqrt{D_0R}} \sqrt{\frac{u_0^2}{4D_0R} + p}\right) + B \exp\left(\frac{zu_0}{2D_0R} - \frac{z}{\sqrt{D_0R}} \sqrt{\frac{u_0^2}{4D_0R} + p}\right) \tag{28}$$

$A = 0$ can be calculated by substituting Equations (23) and (24). With $B = C_0/p$, eventually,

$$C^*(z, p) = \frac{C_0}{p} \exp\left(\frac{zu_0}{2D_0R} - \frac{z}{\sqrt{D_0R}} \sqrt{\frac{u_0^2}{4D_0R} + p}\right) \tag{29}$$

In order to find $C(z, T^*)$, an inversion of $C^*(z, p)$ is required. From the inversion equation, it follows that

$$C(z, T^*) = \frac{1}{2\pi i} \int_{\alpha-i\infty}^{\alpha+i\infty} C^*(z, p) \exp(pt) dp = \frac{C_0}{2\pi i} \int_{\alpha-i\infty}^{\alpha+i\infty} \frac{1}{p} \exp\left(\frac{zu_0}{2D_0R}\right) \exp\left(-\frac{z}{\sqrt{D_0R}} \sqrt{\frac{u_0^2}{4D_0R} + p}\right) \exp(pt) dp \tag{30}$$

This is because

$$L\{\exp(bt^2)f(t)\} = \int_0^\infty \exp(bt^2) \exp(-pt) dt = F\{p - b^2\} \tag{31}$$

So,

$$L^{(-1)}\{F(p - b^2)\} = \exp(bt^2)f(t) = \exp(bt^2)L^{(-1)}\{F(p)\} \tag{32}$$

where $L^{(-1)}$ is the Laplace inversion of L , that is,

$$L^{(-1)}\left\{\exp\left(-\frac{z}{\sqrt{D_0R}} \sqrt{\frac{u_0^2}{4D_0R} + p}\right)\right\} = \exp\left(-\frac{u_0^2}{4D_0R}\right) L^{(-1)}\left\{\frac{z}{\sqrt{D_0R}} \sqrt{p}\right\} \tag{33}$$

So,

$$L^{(-1)}\left\{\frac{z}{\sqrt{D_0R}} \sqrt{p}\right\} = \frac{1}{2\sqrt{\pi T^*}^3} \frac{z}{\sqrt{D_0R}} \exp\left(-\frac{z^2}{4T^*D_0R}\right) \tag{34}$$

The following convolution theorem is used:

$$L^{(-1)}\{F_1(p) \times F_2(p)\} = f_1(t) * f_2(t) \tag{35}$$

where

$$F_1(p) = \frac{1}{p} \tag{36}$$

$$F_2(p) = \exp\left(-\frac{z}{\sqrt{D_0R}} \sqrt{\frac{u_0^2}{4D_0R} + p}\right) \tag{37}$$

Here, $t > 0, t - \tau > 0$, that is, $0 < \tau < t$.

$$L^{(-1)}\left[\frac{1}{p} \exp\left(-\frac{z}{\sqrt{D_0R}} \sqrt{\frac{u_0^2}{4D_0R} + p}\right)\right] = \int_0^t \frac{z}{2\sqrt{D_0R}\pi\tau^3} \exp\left(-\frac{u_0^2}{D_0R\tau} - \frac{u_0^2}{4D_0R}\tau\right) d\tau = \exp\left(-\frac{zu_0}{\sqrt{2D_0R}^2}\right) \int_0^t \frac{\frac{z}{\sqrt{D_0R}} + \frac{u_0\tau}{\sqrt{D_0R}}}{4\sqrt{D_0R}\pi\tau^3} \exp\left(-\frac{\left(\frac{z}{\sqrt{D_0R}} - \frac{u_0\tau}{\sqrt{D_0R}}\right)^2}{4\tau}\right) d\tau + \exp\left(\frac{zu_0}{\sqrt{2D_0R}^2}\right) \int_0^t \frac{\frac{z}{\sqrt{D_0R}} - \frac{u_0\tau}{\sqrt{D_0R}}}{4\sqrt{D_0R}\pi\tau^3} \exp\left(-\frac{\left(\frac{z}{\sqrt{D_0R}} + \frac{u_0\tau}{\sqrt{D_0R}}\right)^2}{4\tau}\right) d\tau \tag{38}$$

In addition,

$$\xi = \frac{Z}{\sqrt{D_0R}} - \frac{u_0\tau}{\sqrt{D_0R}}; \eta = \frac{Z}{\sqrt{D_0R}} + \frac{u_0\tau}{\sqrt{D_0R}} \tag{39}$$

The error function is introduced, and then the result is substituted into the original equation to obtain the final analytical solution.

$$C(z, T^*) = \frac{C_0}{2} \exp\left(\frac{u_0z}{2D_0R} - \frac{u_0^2T^*}{4D_0R}\right) \left[\exp\left(\frac{u_0^2T^*}{4D_0R} - \frac{u_0z}{2D_0R}\right) \operatorname{erfc}\left(\frac{Rz}{2\sqrt{D_0T^*R}} - \frac{u_0T^*}{2\sqrt{D_0T^*R}}\right) + \exp\left(\frac{u_0^2T^*}{4D_0R} + \frac{u_0z}{2D_0R}\right) \operatorname{erfc}\left(\frac{Rz}{2\sqrt{D_0T^*R}} + \frac{u_0T^*}{2\sqrt{D_0T^*R}}\right)\right] \tag{40}$$

The new time variable obtained with Equation (13) has the following expression:

$$T^* = t + at^2/2 \quad (41)$$

3. Verification

The analytical solution in this study is based on neglecting the effect of the effective molecular diffusion coefficient, and the solution in this study can be degraded to a constant-flow-rate analytical solution [40] as follows:

$$C(z, t) = \frac{C_0}{2} \left[\operatorname{erfc} \left(\frac{Rz}{2\sqrt{D_0 t R}} - \frac{u_0 t}{2\sqrt{D_0 t R}} \right) + \exp \left(\frac{u_0 z}{D_0} \right) \operatorname{erfc} \left(\frac{Rz}{2\sqrt{D_0 t R}} + \frac{u_0 t}{2\sqrt{D_0 t R}} \right) \right] \quad (42)$$

This solution is compared with the analytical solution in this study to illustrate the rationality of the model. The values of the parameters are as follows: the hydrodynamic dispersion coefficient is $D_h = 3 \times 10^{-9} \text{ m}^2/\text{s}$, the convective initial velocity is $u_0 = 3 \times 10^{-8} \text{ m/s}$, the maximum flow rate reached is $v_e = 1.44 \times 10^{-7} \text{ m/s}$, the influence coefficient is $a = 1.46 \times 10^{-8} / \text{s}$, the initial concentration of pollutants is $C_0 = 1 \text{ mg/L}$, the retention factor is $R = 20$, and the depth is $L = 1 \text{ m}$.

Figure 1 shows that the degenerated constant-velocity solution in this study is in good agreement with the solution in [40], which demonstrates the correctness of the one-dimensional variable-velocity contaminant transport equation solved in this study.

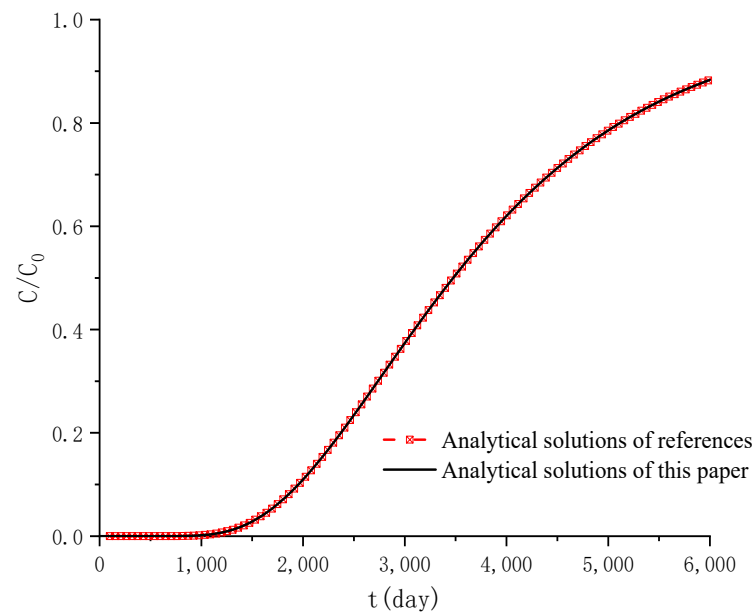


Figure 1. Comparison of the outflow curves between the present solution and the analytical solution.

The numerical solution considering the molecular diffusion D^* was analyzed by using the Geo-studio numerical simulation software. The numerical solution was also used for a comparison with the solution in this study. The molecular diffusion here is $D^* = 3.45 \times 10^{-10} \text{ m}^2/\text{s}$.

The Péclet number Pe is a factor-free parameter representing the ratio of convectivity to diffusivity. $Pe = u_0 L / D_h$. The molecular diffusion is so small that it can be ignored.

Specifying a breakthrough concentration of 10%, Figure 2 shows the effects of considering molecular diffusion and not considering molecular diffusion on the breakthrough time. It can be clearly seen that effective molecular diffusion had a very small effect of 3.9% on the scenarios that were analyzed in this section. All Pe values in the subsequent studies in this paper are greater than those in this section. This suggests that the assumption of ignoring effective molecular diffusion is feasible and provides theoretical support for the subsequent analysis.

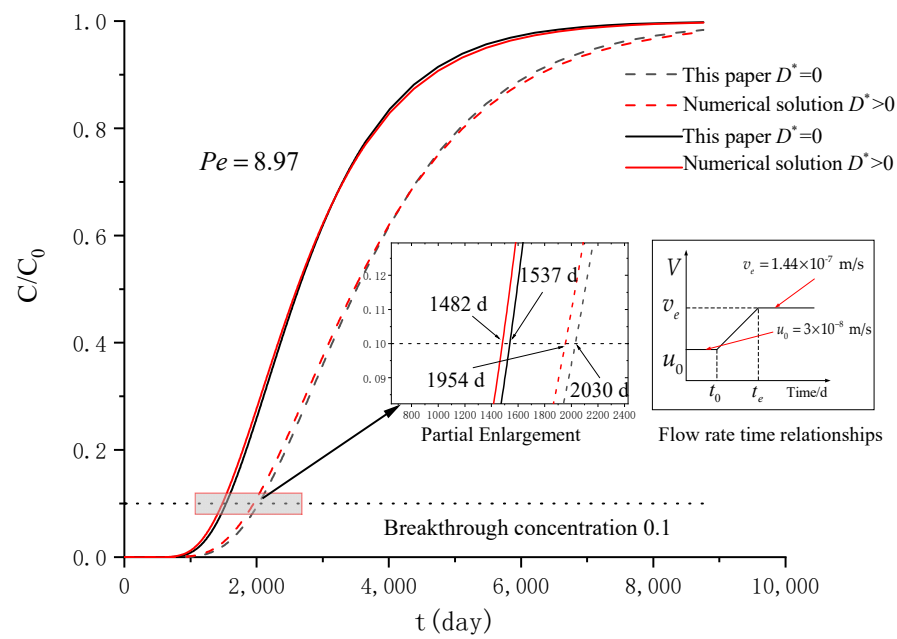


Figure 2. Comparison with numerical solutions.

4. Parameter Impact Analysis

The following is a comparative analysis of the variable-flow-velocity migration mechanisms of the contaminants for which solutions were found in this study in combination with different parameters. The main considerations were the magnitude of the flow velocity, the time required to reach the maximum flow velocity, and the effect of the influence coefficient on the migration of pollutants. The analysis was divided into three working conditions, namely:

- (1) Influence coefficient a varies, maximum velocity v_e varies, and the time to maximum velocity t_e is constant.
- (2) Influence coefficient a varies, maximum velocity v_e is constant, and the time to maximum velocity t_e varies.
- (3) Influence coefficient a is constant, maximum velocity v_e varies, and the time to maximum velocity t_e varies.

According to [31,41], the parameters sets for the groups are shown in Table 1.

Table 1. Calculation and analysis scheme and parameter values.

Group	Case	a (s^{-1})	v_e (m/s)	t_e (d)
1	1-1	1.46×10^{-8}	6.78×10^{-8}	1365
	1-2	2.01×10^{-8}	1.06×10^{-7}	1365
	1-3	3.23×10^{-8}	1.44×10^{-7}	1365
2	2-1	4.39×10^{-8}	1.44×10^{-7}	1365
	2-2	2.19×10^{-8}	1.44×10^{-7}	2365
	2-3	1.46×10^{-8}	1.44×10^{-7}	3365
3	3-1	1.46×10^{-8}	6.78×10^{-8}	1365
	3-2	1.46×10^{-8}	1.06×10^{-7}	2365
	3-3	1.46×10^{-8}	1.44×10^{-7}	3365

The parameters of the conventional model are shown in Table 2.

Table 2. Calculation parameters of the conventional model.

Parameter Value	
Partition coefficient k_p	7.5 mL/g
Height L	1 m
Hydraulic gradient i	5
Dispersion α	0.1 m
Porosity n	0.5
Permeability coefficient k_s	3×10^{-9} m/s
t_0	365/d
u_0	3×10^{-8} m/s
D_h	3×10^{-9} m ² /s
R	20

4.1. Analysis of Parameter Influence in Group 1

Figure 3 shows the velocity over time for the simulations in Group 1. In practice, this can be used to evaluate barriers with different degrees of deterioration over the same period of time. The breakthrough time when $C/C_0 = 0.1$ is evaluated for each case.

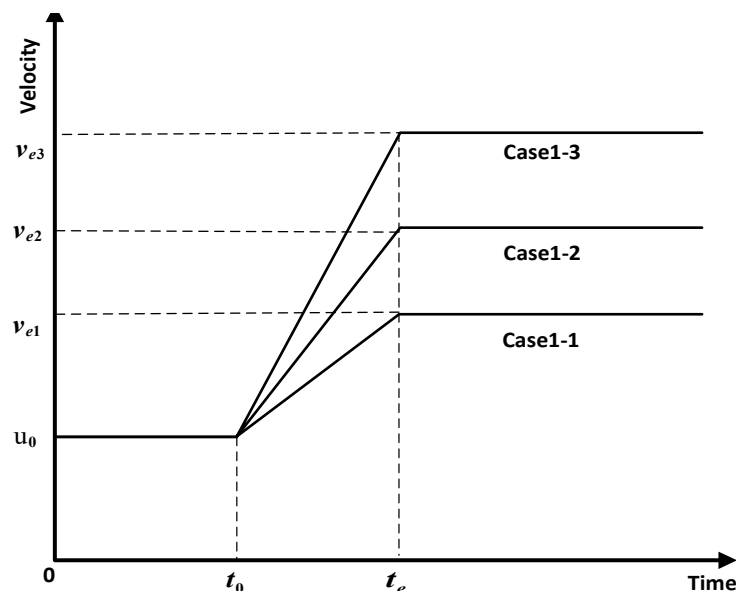


Figure 3. Velocity–time relationships in Group 1.

Figure 4 is the outflow curve for Group 1, combined with $u_0 = 3 \times 10^{-8}$ m/s and $v_e = 1.44 \times 10^{-7}$ m/s. The breakthrough times corresponding to the above constant-flow-rate migration are 4059.308 d and 1217.779 d, respectively. A breakthrough occurs earliest in Case 1-3, and the breakthrough time is $t_{1-3} = 1707.156$ d. Cases 1-2 and 1-1 are followed by a breakthrough. The breakthrough times are $t_{1-2} = 2030.348$ d and $t_{1-1} = 2274.864$ d. Cases 1-3 and the constant flow rate u_0 result in a breakthrough time difference of $t_{1-3} - t_0 = 2352.152$ d; Case 1-2 and the constant flow rate u_0 result in a breakthrough time difference of $t_{1-2} - t_0 = 2028.96$ d. Case 1-1 and the constant flow rate u_0 result in a breakthrough time difference of $t_{1-1} - t_0 = 1784.444$ d. It can be seen that the breakthrough time for variable-flow-rate pollutant migration is reduced from 11 years to between 4 and 6 years as the influence coefficient is expanded for a constant time. Comparing the influence coefficient a , the influence coefficient for Case 1-3 is twice that of Case 1-1, and according to Equation (5), the flow rate is correspondingly expanded by a factor of two, thus reducing the breakthrough time by 567.708 d. The influence coefficient a for Case 1-2 is 1.6 times that of Case 1-1, and the flow rate is correspondingly expanded by a factor of 1.4, thus reducing the breakthrough time by 323.19 d.

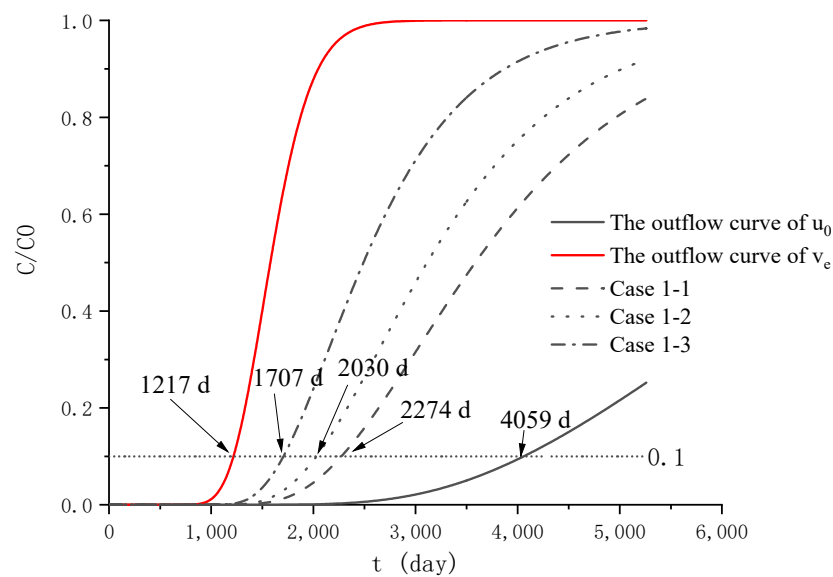


Figure 4. Outflow curves for Group 1.

Figure 5 shows the concentration difference between the constant and variable flow rates for Group 1. The difference in concentration occurs because the outflow curve is convergent, the flow rate gradually increases from the initial value to the maximum value, and the difference in concentration first gradually increases and then begins to decrease after reaching the peak. In Group 1, the velocity increment in Case 1-1 is the smallest, the differential concentration curve is gentle, the peak time appears late, and the peak is small; the velocity increment in Case 1-3 is the largest, the differential concentration curve is the steepest, the peak time appears early, and the peak is large. The analysis in Figure 5 shows that the steeper the flow velocity curve is, the shorter the time required to reach the peak is, and the larger the peak concentration difference is, and the smoother the difference curve is for smaller flow velocities, the longer the time required to reach the peak and the smaller the corresponding peak concentration difference. This shows that the effects of the influence coefficient a on the transport of pollutants are very significant.

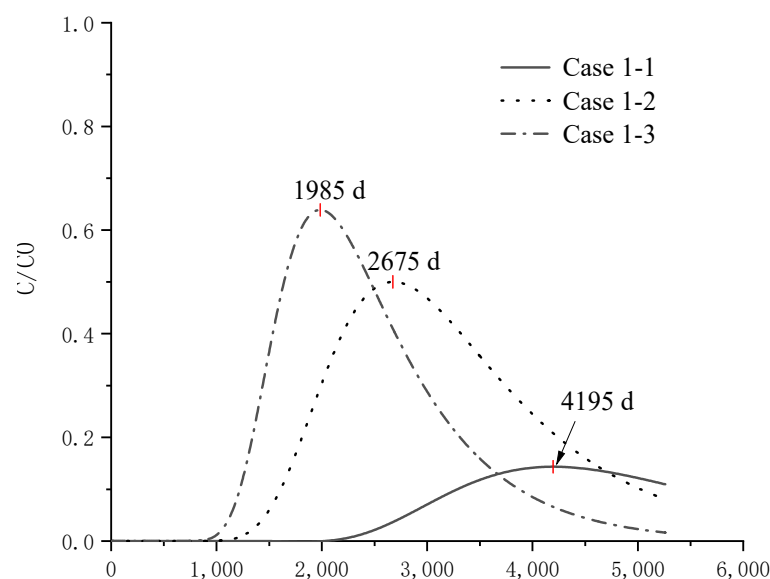


Figure 5. Difference in concentration between the constant and variable flow rates in Group 1.

Figure 6 shows the concentration profiles of contaminant migration for Case 1 versus the constant flow rate. At 2365 d, Case 1 both reached the maximum velocity and both had

a breakthrough; according to Figure 6, the difference in contaminant concentration between the cases increased with depth, and the influence of coefficient a on the contaminant concentration was significant, with a two-fold difference in the influence coefficient a between Case 1-1 and Case 1-3 and a two-fold difference in the contaminant concentrations, which differed by a factor of 4.

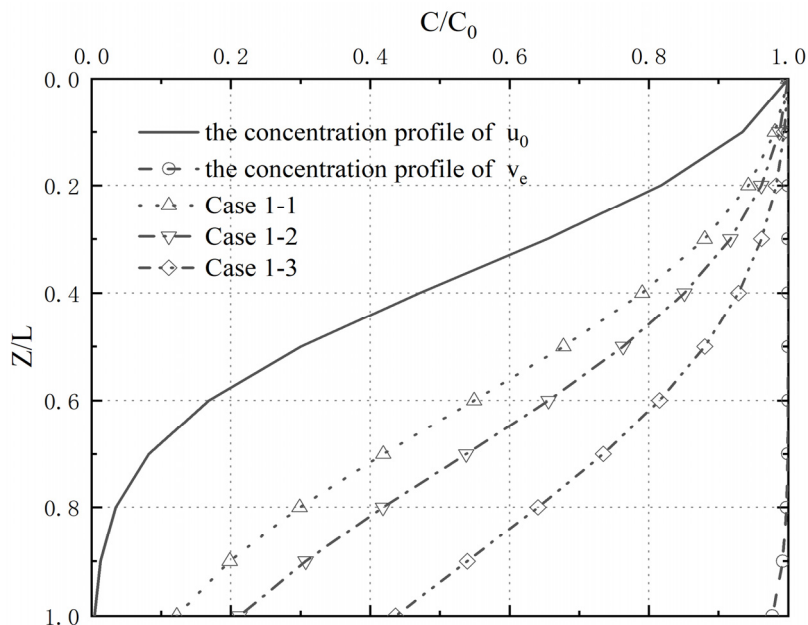


Figure 6. Concentration profiles of Group 1.

4.2. Analysis of Parameter Influence in Group 2

Figure 7 shows the velocity over time for the simulations in Group 2. In practice, this can be used to evaluate barriers with the same degree of deterioration and different deterioration development times, i.e., to evaluate the service performance of the same barrier with different sources of pollution and under different geological conditions. The breakthrough time when $C/C_0 = 0.1$ is evaluated for each case.

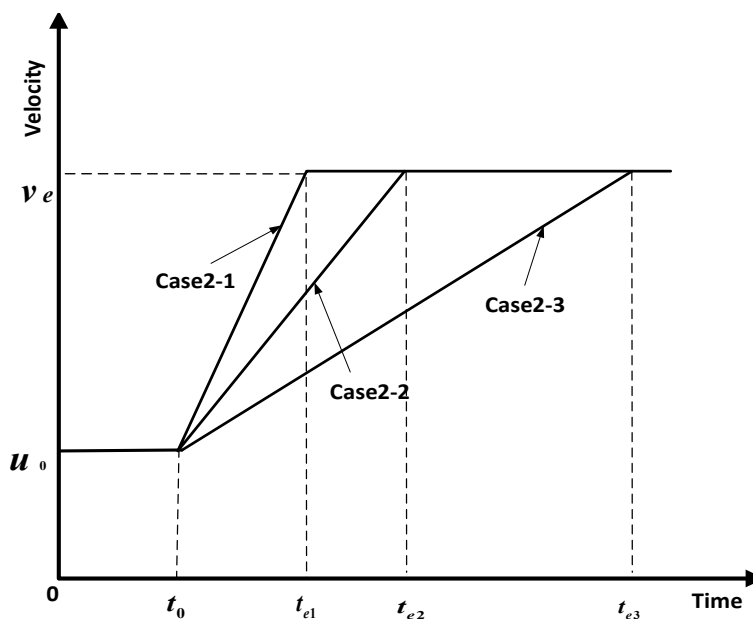


Figure 7. Velocity–time relationships in Group 2.

Figure 8 shows the outflow curve for Group 2 combined with $u_0 = 3 \times 10^{-8}$ m/s and $v_e = 1.44 \times 10^{-7}$ m/s. The breakthrough times corresponding to the migration at a constant flow velocity are 4059.308 d and 1217.779 d, respectively. Case 2-1 is the first to start breakthrough; here, the breakthrough time is $t_{2-1} = 1531.214$ d. Secondly, a breakthrough begins at $t_{2-2} = 1880.231$ d in Case 2-2. The last breakthrough starts in Case 2-3 at a breakthrough time of $t_{2-3} = 2116.878$ d. Case 2-3 and the constant flow rate v_{e3} result in a breakthrough time difference of $t_0 - t_{2-3} = 1942.43$ d. Case 1-2 and the constant flow rate v_{e2} result in a breakthrough time difference of $t_0 - t_{2-2} = 2179.077$ d. Case 1-1 and the constant flow rate v_{e1} result in a breakthrough time difference of $t_0 - t_{2-1} = 2528.094$ d. It can be seen that at a constant maximum velocity, the breakthrough time increases as the influence coefficient a decreases. In comparison with the constant-flow-rate case, the breakthrough time is reduced from 11 years to 4 to 6 years. Comparing the influence coefficient a , that in Case 2-1 is three times larger than that in Case 2-3, with a corresponding three-fold expansion in velocity according to Equation (5) and an increase in breakthrough time of 585.664 d. That in Case 2-1 is two times larger than that in Case 2-2, with a corresponding two-fold expansion in velocity according to Equation (5) and an increase in breakthrough time of 349.017 d. Compared to Case 1, Case 2 gives the maximum velocity and changes the time. In this case, the breakthrough time is significantly earlier than that in Case 1.

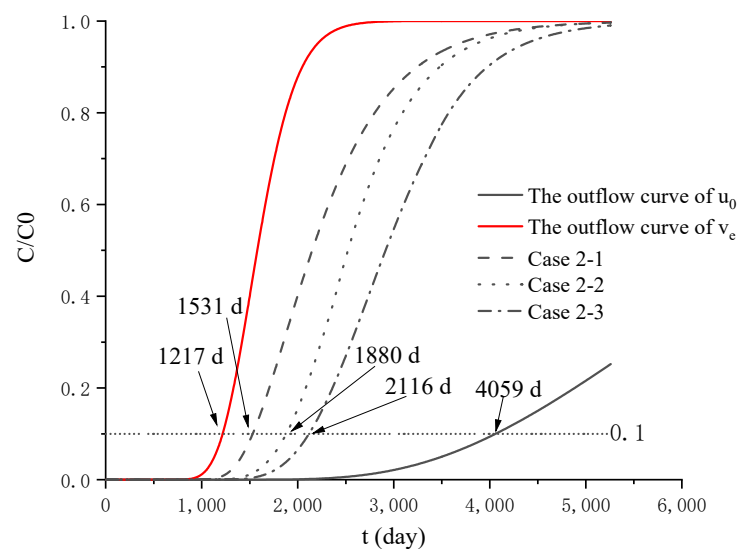


Figure 8. Outflow curves of Group 2.

Figure 9 shows the concentration differences between Group 2 and the constant flow migration, where it is clear that the concentration differences first increase with the same trend and then reach the peak concentration differences. Unlike Group 1, Group 2 has the same maximum velocity, and only the time and influence coefficient a are changed. The peaks are more concentrated at this point, but the peak concentrations are both greater than those with Condition 1, and the curves are both steeper. It can be seen that the effect of this condition on the peak occurrence time of the variable-flow-rate pollutant migration is very small, and the effect on the peak is larger.

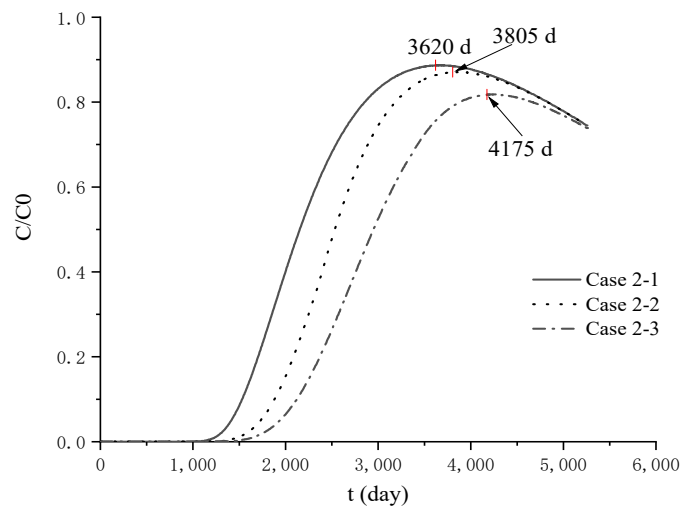


Figure 9. Difference in concentration between the constant and variable flow rates in Group 2.

4.3. Analysis of Parameter Influence in Group 3

Figure 10 shows the velocity over time for the simulations in Group 3. In practice, it is possible to represent situations in which the same barrier experiences different times of deterioration. The breakthrough time when $C/C_0 = 0.1$ is evaluated for each case.

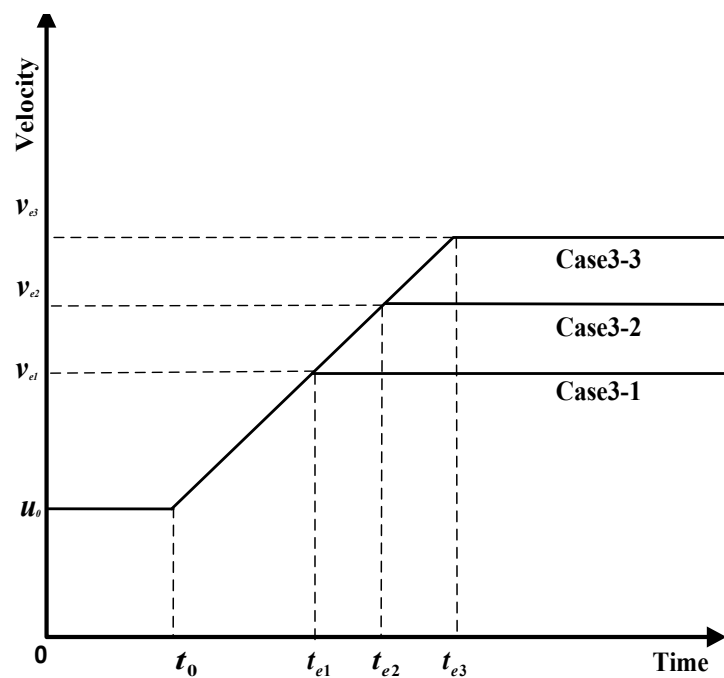


Figure 10. Velocity–time relationships in Group 3.

Figure 11 shows the outflow curve for Group 3 combined with $u_0 = 3 \times 10^{-8}$ m/s and $v_e = 1.44 \times 10^{-7}$ m/s. The breakthrough times corresponding to the migration at a constant flow velocity are 4059.308 d and 1217.779 d, respectively. The breakthrough starts earliest in Case 3-2 and Case 3-3, and the breakthrough time is $t_{3-2,3-3} = 2116.878$ d. A breakthrough occurs at $t_{3-1} = 2274.864$ d in Case 3-1. The breakthrough starts latest in Case 2-3, and the breakthrough time is $t_{3-3} = 2116.878$ d. As can be seen in Figure 11, because the influence coefficients a are equal, the outflow curves of Group 3 before 1365 d overlap, the image of Case 3-2 appears after 1365 d, and the image of Case 3-3 appears after 2365 d. This shows that the influence coefficient determines the magnitude of the change in the outflow curve images.

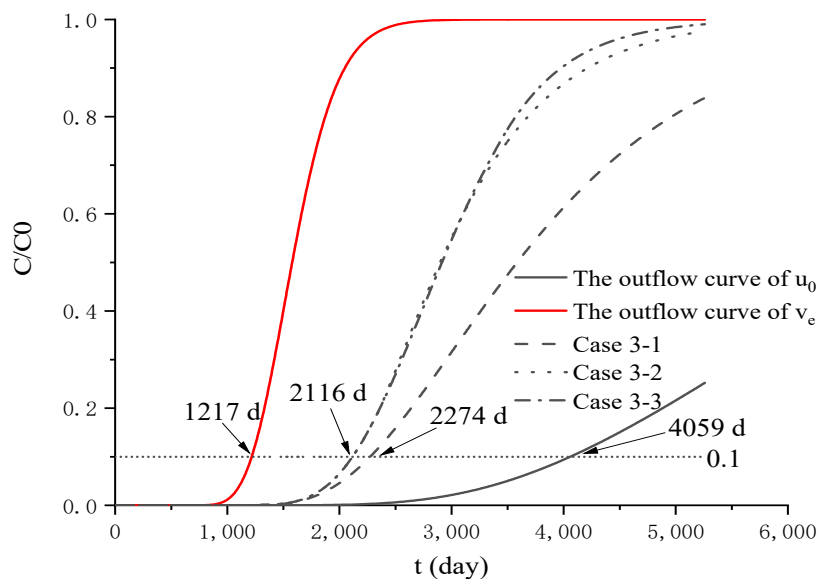


Figure 11. Outflow curves of Group 3.

Figure 12 shows the concentration difference between the three cases in Group 3 and the constant-flow-rate migration. As in Group 1, the concentration difference first gradually increases, and after reaching the maximum concentration difference peak, the concentration difference starts to gradually decrease. The velocity increment in Group 3 is constant and the time changes, making it a combination of Group 1 and Group 2. The general rule is the same as that for Group 1, except that the difference in the maximum flow rate results in a different peak concentration. It can be seen that the peak concentrations occur for different cases, and the larger the value of a is, the larger the peak difference, the steeper the curve, and the earlier the peak concentration difference.

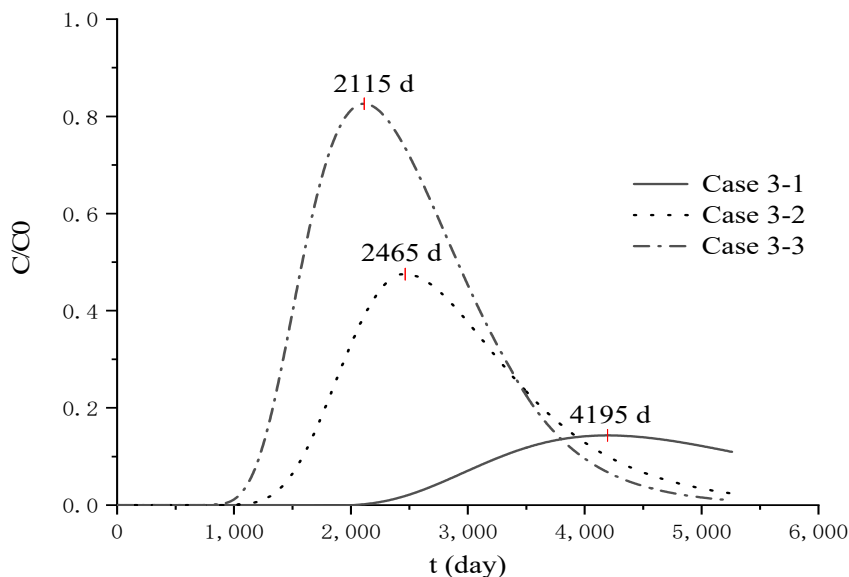


Figure 12. Difference in concentration between the constant and variable flow rates in Group 3.

Figure 13 shows the concentration profile of the contaminant migration for Group 3 and the constant flow rate. At 2365 d, Case 3-2 just reaches the maximum velocity, and Case 3-3 also reaches the same velocity, so the curve of Case 3-2 coincides with the curve of Case 3-3. In addition, Group 3 can be considered a combination of Group 1 and Group 2. It is clear that the profile concentration with the variable flow velocity is significantly greater than the profile concentration with the initial velocity and less than the profile

concentration with the maximum velocity; the images are between the initial and maximum velocity images.

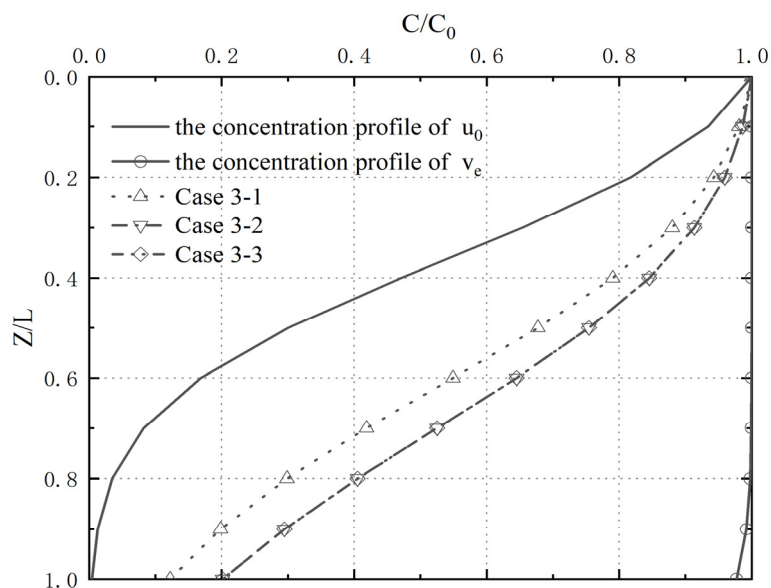


Figure 13. Contaminant migration profile in Group 3.

4.4. Analysis of Pollutant Concentration Differences

The contaminant migration concentrations with a variable flow rate and constant flow rate in the above three cases are compared and analyzed, and the abscissa of Group 1 and Group 2 is the influence coefficient a . The abscissa of Group 3 is the maximum flow rate. The ordinate of the image is the contaminant concentration difference and the time required to reach the peak concentration difference.

The migration concentrations of pollutants at variable flow rates are analyzed against the normal flow rate for each of the three conditions, with the influence coefficient a in the horizontal coordinates of Group 1 and Group 2 (Figure 14a) and the maximum flow rate in the horizontal coordinate of Group 3 (Figure 14b). The vertical coordinates of the images are the difference in pollutant concentration and the time taken to reach the peak concentration difference, respectively.

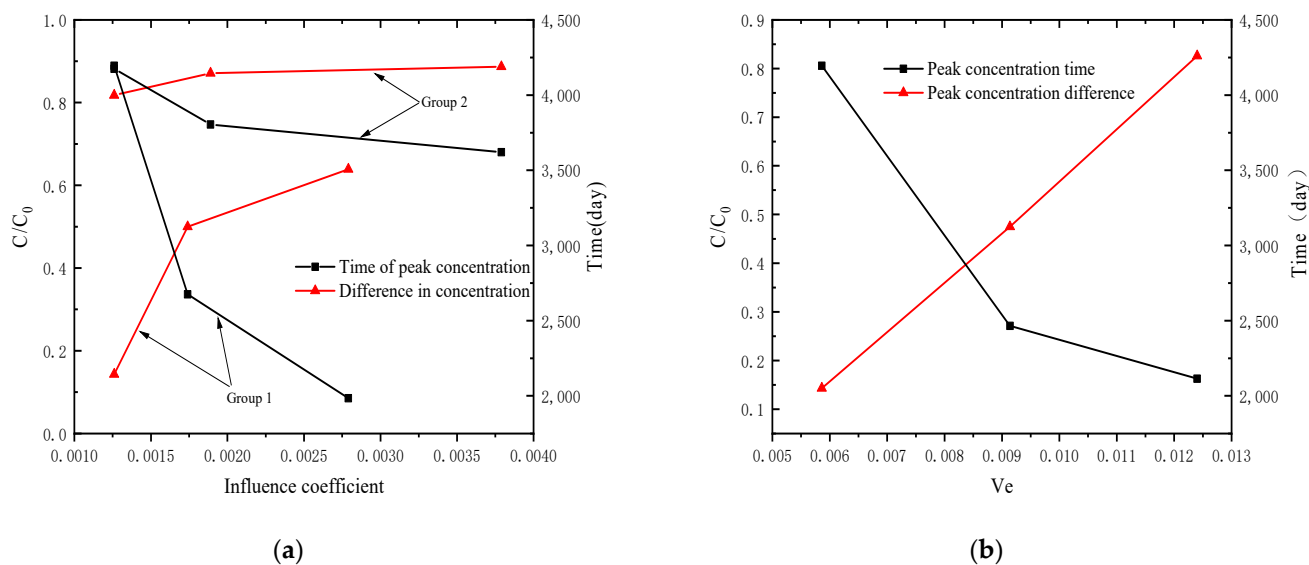


Figure 14. Peak concentration relationships. (a) Relationship between peak concentration and influence coefficient. (b) Relationship between peak concentration and maximum flow velocity.

We already know that there is a difference in concentration between the constant- and variable-flow-rate migration of pollutants and that this difference will peak at a certain point and at a certain depth. It is clear that the time taken to reach the peak concentration difference decreases as the influence coefficient and maximum flow rate increase for all three conditions, and it is clear that the time taken to reach the peak concentration difference increases as the influence coefficient a and maximum flow rate increase for all three conditions. This indicates that the level of pollutant concentration inside the barrier increases significantly when changes in flow velocity are taken into account, which seriously affects the performance of the barrier. In engineering practice, it is difficult to fully consider the effect of flow velocity variation. We can consider predicting the concentration of pollutants in the general normal-flow-rate migration of pollutants in a barrier system first, and then judge the pollutant concentration level inside the barrier system according to the difference in pollutant concentrations between the variable flow rate and the normal flow rate.

From the above analysis, it is clear that variable-flow-rate migration is important for pollutant migration control, and the influence coefficient a determines the variable-flow-rate migration of pollutants. Considering the variable-flow-rate situation, the concentration level of pollutants increases, and changing the influence coefficient a can reduce the rate of pollutant migration. Often, reducing a by a factor of 2 can reduce the concentration of pollutants by a factor of 4, which can significantly improve the antifouling performance of materials for porous media.

It is clear that the time required to reach the peak concentration difference gradually increases with the increase in the influence coefficient a and maximum flow velocity for all three operating cases. This shows that the level of contaminant concentration inside the barrier significantly increases when considering changes in flow velocity, which seriously affects the performance of the barrier in service.

From the above analysis, it can be seen that variable-velocity migration is very important for the prevention and control of contaminant migration, and the influence coefficient a determines the variable-velocity migration of pollutants. Considering a variable flow rate, when the contaminant concentration level increases, changing the influence coefficient a can reduce the contaminant migration rates. Often, reducing the influence coefficient a by two times can reduce the contaminant concentration by four times, thus significantly improving the antifouling performance of materials for porous media.

5. Example Analysis

5.1. Analysis of a Soil–Attapulgite Barrier

For this analysis, the parameter values were taken from [2,42–47], and the ion concentration of the heavy metal pollutant Co^{2+} was studied. With the confining pressure of 100 kpa, the analysis was carried out in three cases according to different mixing proportions of attapulgite (A) and sand (S). At a temperature of 30–60 °C, the permeability coefficient k_s of the wall was basically in the range of $0 \sim 4 \times 10^{-9}$ m/s, the liquid limit of attapulgite was $W_1 = 11.41\%$, the plastic limit was $W_p = 5.6\%$, the dry density was $\rho = 808 \text{ kg/m}^3$, the porosity was $n = 0.2 \sim 0.64$, the distribution coefficient was $k_d = 43 \text{ mL/g}$, the barrier thickness was $L = 1 \text{ m}$, and $t = 280 \text{ d}$ for the temperature of the landfill to rise from 30 °C to 60 °C under the action of biodegradation, that is, it took 280 d to reach the maximum velocity. From $u(t) = u_0 V(at)$, we obtained a .

The percentages of attapulgite in the mix were set to 10%, 30%, and 60%. The values of the relevant parameters are shown in Table 3. The antifouling effect of the soil–attapulgite barrier was compared in the cases of variable flow velocity and constant flow velocity.

Table 3. Analysis cases and parameter values.

Case	Ratio %	Porosity	Permeability Coefficient m/s		a	R
			30 °C	60 °C		
1	A10S90	0.286	1.66×10^{-9}	3.32×10^{-9}	0.0036	81
2	A30S70	0.405	1.02×10^{-9}	2.64×10^{-9}	0.0056	61
3	A60S40	0.5	2.22×10^{-10}	6.54×10^{-10}	0.0068	49

Figure 15 shows the partial enlargement of the contaminant concentration, which allowed curves corresponding to the defined 10% breakthrough concentration in cases 1, 2, and 3 to show the breakthrough time of the heavy metal ion Co^{2+} for the barrier.

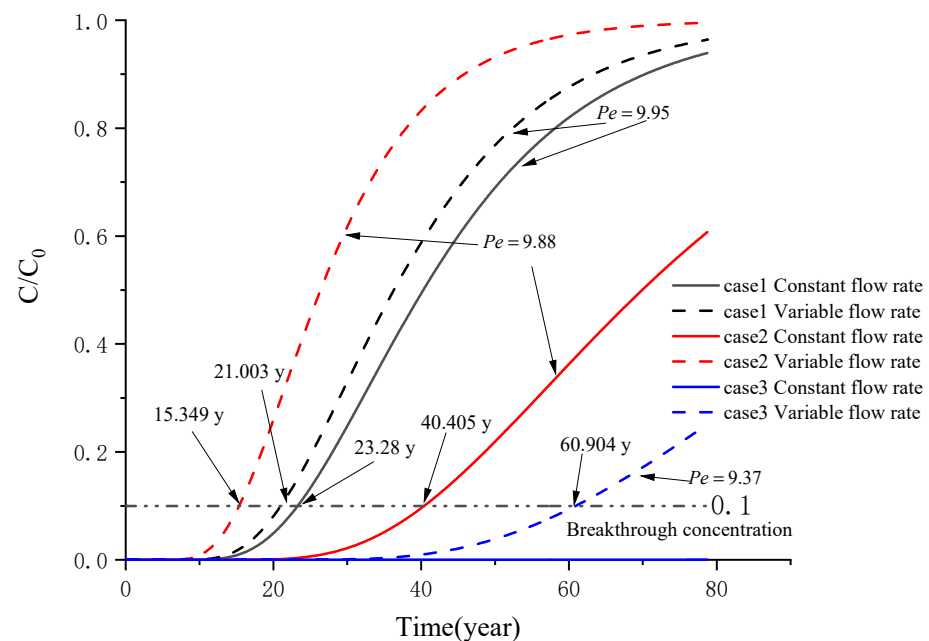


Figure 15. Outflow curve of the soil-attapulgite barrier.

As can be seen in Figure 15, the breakthrough times of the barrier were compared for the variable- and constant-flow-rate migration of contaminants in Cases 1, 2, and 3. The Pelect values obtained for the parameters that were used were all greater than the Pelect values in Section 3, indicating that the influence of molecular diffusion could be ignored.

Case 1, with 10% attapulgite, migrated at an initial pollutant flow velocity of $u_1 = 2.75 \times 10^{-8}$ m/s and reached a maximum flow velocity of $u_{e1} = 5.52 \times 10^{-8}$ m/s at 280 d, with a breakthrough of 21.003 y, compared to 23.28 y for the constant-flow-velocity case. Case 2, with 30% attapulgite, had an initial velocity of pollutant flow of $u_2 = 1.18 \times 10^{-8}$ m/s, and it took 280 d to reach the maximum flow velocity $u_{e2} = 3.30 \times 10^{-8}$ m/s for migration. A breakthrough time of 15.349 years was obtained for the variable flow rate and a value of 40.045 years was obtained for the constant flow rate. The initial flow rate for Case 3 was $u_3 = 2.22 \times 10^{-9}$ m/s. The breakthrough time of the barrier under the influence of the variable flow rate was 60.904 years; at this point, the migration of contaminants at the constant flow rate did not occur as a breakthrough.

Comparing the breakthrough times of the soil-attapulgite barrier, it was clear that the greater the attapulgite admixture, the better the soil-attapulgite barrier was at keeping out contaminants. Comparing the effects of the permeability coefficient, it was difficult for a breakthrough to occur in the barrier at a constant flow rate (constant landfill temperature), but as the landfill temperature increased, the permeability coefficient gradually increased, with a breakthrough time of 21.003 y in Case 1, which was a reduction of 9.8% compared to the constant flow rate. Case 2 had a breakthrough time of 15.349 y, which was a reduction of 62.01% compared to the constant flow rate. Case 3 had no concentration at the constant

flow rate for 80 years, but the breakthrough time under the influence of the variable flow rate occurred at 60.904 years. This showed that the increase in the permeability coefficient of the barrier caused by the increase in landfill temperature could significantly reduce the soil–attapulgite fouling performance.

Figure 16 shows the contaminant concentration distribution of the attapulgite barrier with different contents in Cases 1, 2, and 3 at $t = 30$ y. In the case of a constant flow rate, the concentration of Co^{2+} ions in the lower layer gradually decreased with the increase in the doping amount. By comparing the variable flow rate with the constant flow rate, it can be seen that the increase in the permeability coefficient of the barrier caused by the increase in the landfill temperature weakened the barrier capacity.

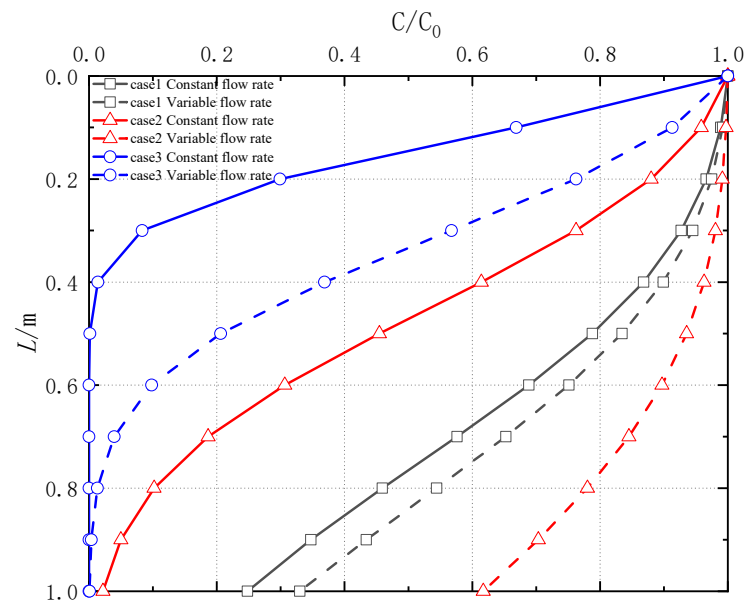


Figure 16. Concentration profile of the soil–attapulgite barrier.

The ion concentration of Co^{2+} in the lower layer of the barrier became smaller; the concentration at the bottom in the 10% case was the highest, and was 0.27 different from that in the 60% case. This showed that with the increase in attapulgite content, the adsorption capacity of the lower layer of the partition barrier became larger, but the main factor affecting the decrease in its concentration was not the change in the retardation factor because the retardation factor R and permeability coefficient became smaller with the increase in attapulgite content; $R = 81$ at 10%, $R = 61$ at 30%, and $R = 49$ at 60%. At the same time, the flow rate was also gradually reduced, so it can be seen that in this case of contaminant migration, the concentration change was dominated by the flow rate, so it was not necessary for the adsorption capacity to be strong when the retardation factor was large, and more attention should be paid to the permeability of the barrier. In engineering practice, measures such as increasing the content of attapulgite and controlling the temperatures of landfills can enhance barriers' effects.

5.2. Analysis of a Sand–Bentonite Mixture (SBM) Barrier

Fan Ridong [48] successively tested the permeability coefficients of SBM specimens under the continuous action of three concentrations of lead nitrate–zinc nitrate solutions and found that the permeability coefficient increased with the increase in pore volume at each concentration, and the greater the concentration, the greater the value of the final stable permeability coefficient. $\text{Pb}(\text{NO}_3)_2$ – $\text{Zn}(\text{NO}_3)_2$ with initial metal concentrations C_0 of 50, 100, and 500 mmol/L, a retardation factor of $R = 10$, and $z = 1$ m were selected, and the measured permeability coefficients were 4.1×10^{-10} m/s, 3.5×10^{-9} m/s, and 5×10^{-9} m/s, which increased to 3.8×10^{-9} m/s, 5.5×10^{-9} m/s, and 7.4×10^{-9} m/s after one year, with influence coefficients of $a_1 = 2.67 \times 10^{-7}$, $a_2 = 1.81 \times 10^{-8}$, and $a_3 = 1.52 \times 10^{-8}$, respec-

tively. The breakthrough criterion was a contaminant concentration at the lower boundary of 10% of that of the upper boundary.

Figure 17 shows the outflow curves for three concentrations of Pb-Zn nitrate solutions. The Péclet values obtained for the parameters that were used were all greater than the Péclet values in Section 3, indicating that the influence of molecular diffusion could be ignored. Compared to the results of the uncontaminated test, the permeability coefficients increased by factors of 9.3, 1.6, and 1.48 for the different concentrations of lead nitrate and zinc nitrate solutions. The breakthrough time of the SBM barrier was reduced by 2.608 years, 1.699 years, and 1.29 years, respectively, with 28.7% and 22.7% reductions in the breakthrough time for the 100 mmol/L and 500 mmol/L Pb-Zn contaminant concentrations, respectively. The concentration of the 50 mmol/L Pb-Zn solution at 14 years under constant-flow-rate migration was very low, and no breakthrough occurred.

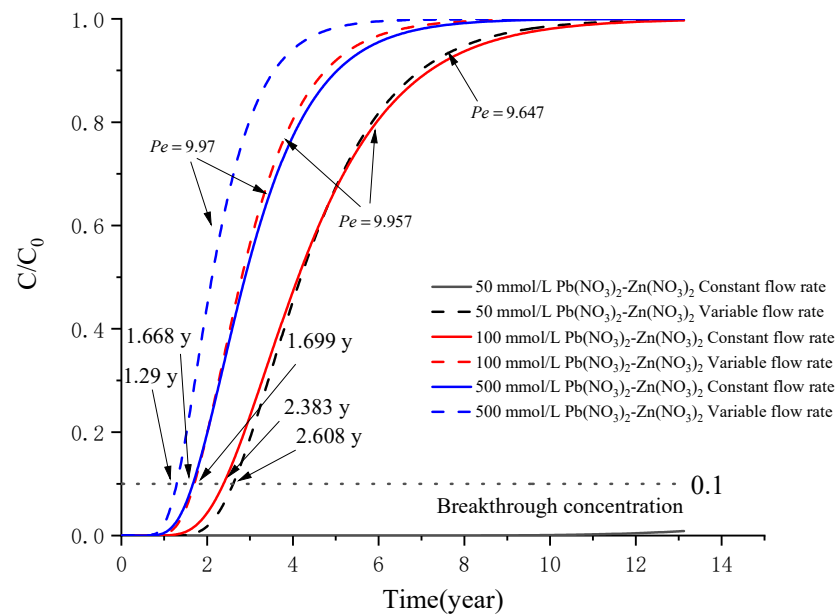


Figure 17. The outflow curves for the 10% concentration.

The above results indicate that the permeability coefficient of the sand–bentonite barrier increased linearly with the increase in the metal concentration in the presence of the heavy metal Pb-Zn composite solution, resulting in an increase in the flow rate of contaminant migration and a reduction in the breakthrough time of the heavy metal contaminants. This suggests that in areas where Pb-Zn is the dominant heavy metal contaminant, a change in the permeability coefficient has a greater impact on the service performance of a sand–bentonite barrier.

6. Conclusions

In this study, a one-dimensional model was proposed to simulate the transport of relatively complex pollutants through a barrier by considering the changes in pollutant velocity over time. On the basis of this model, analytical solutions were obtained. Based on this solution, the following conclusions are drawn.

The solution of the variable-flow-rate analysis in this study can be downgraded to the solution of a constant-flow-rate analysis. The degraded analytical solution for the constant flow rate was compared with the existing analytical solution, and the results were in complete agreement, indicating that the model was correctly solved. A comparison with the case of considering molecular diffusion showed that the effect of considering molecular diffusion on the solution in this study was very small, which showed the reasonableness of this model.

One-dimensional contaminant migrations with three variable-velocity groups were discussed. Different degrees of deterioration in the barrier occurred at the same time in Group 1. In this group, compared with the normal flow rate, the breakthrough time of the barrier was shortened by about two times if the flow rate was increased by two times. Group 2 represented the same barrier with a different source of pollution and under different geological conditions. Unlike Group 1, Group 2 had the same maximum velocity, changing only the time and the influence coefficient a . The level of contaminant concentration inside the barrier was increased by a factor of 4 when compared with the level with the constant flow rate. Group 3 represented a case in which the same barrier experiences a different time of deterioration. As the influence coefficient a remained constant, the outflow curves occurred sequentially over time, and the longer the barrier had to deteriorate, the greater the flow rate v_e was after equilibrium was reached, and the worse the performance was. All three groups showed that the effect of a variable flow velocity on the migration of pollutants within a barrier was very significant. Increasing v by a factor of 2 resulted in a significant increase in the level of pollutant concentration within the barrier, with the concentration of pollutants within the barrier increasing by a factor of around 4, thus seriously affecting the performance of the barrier. The analysis also showed that there is a concentration difference between the variable- and constant-flow-rate migration of pollutants and that this concentration difference would have a peak concentration difference at a certain time, which was related to t and a . The time t determined when the peak concentration occurred, and the coefficient a determined the size of the maximum concentration difference.

Based on the analytical solution obtained in this study, the migration heavy metal Co^{2+} ions in a soil–attapulgite barrier was analyzed as the temperature of a landfill increased from 30 °C to 60 °C. With the increase in the temperature, the permeability coefficient of the barrier increased. The permeability coefficient and retardation factor decreased with the increase in the content of attapulgite, and the flow rate decreased, so the barrier's effect on the pollutants improved. A breakthrough concentration of 10% was defined. In the case of increasing permeability coefficients with time, the breakthrough time was correspondingly advanced by 9.8% and 62.01%. In engineering practice, measures such as increasing the content of attapulgite and controlling the temperature of a landfill can enhance a barrier's effect.

The performance of the sand–bentonite barrier with Pb–Zn solutions was predicted by using the analytical scheme obtained in this study. The analytical results showed that the chemical compatibility of heavy metal contaminants significantly increased the permeability of the barrier material, leading to a decrease in the performance of the sand–bentonite barrier, with the breakthrough times being advanced by 28.7% and 22.7% with constant permeability coefficients. In practice, the chemical compatibility of a barrier material can be improved by using bentonite modification techniques to improve its performance.

Author Contributions: Study concept and design, X.Z., L.X. and Z.H.; Calculation of the model, X.Z. and T.G.; Validation, T.G.; Analysis of data, T.G.; Interpretation of data, X.Z. and T.G.; Writing manuscript, T.G.; Project administration, X.Z.; Critical revision, All authors. All authors have read and agreed to the published version of the manuscript.

Funding: This research was funded by the National Natural Science Foundation of China (Grant No. 41702329), the Open Research Fund Program of Hunan Provincial Key Laboratory of Geotechnical Engineering for Stability Control and Health Monitoring (Grant No. E22213), and the Natural Science Foundation of Hunan Province, China (Grant No. 2022JJ40148).

Data Availability Statement: The submitted manuscript contains all of the data generated or analyzed throughout this study.

Conflicts of Interest: The authors declare no conflict of interest.

References

1. Zhang, Y.; Xiang, Y.; Chen, W. Heavy metal content in the bark of camphora tree in Xiangtan and its environmental significance. *Appl. Ecol. Environ. Res.* **2019**, *17*, 9827–9835. [[CrossRef](#)]
2. Cao, J.; Zhang, J.; Zhang, W.; Liu, M.; Shi, Z. Research progress of remediation technology for heavy metal chromium(VI) contamination in soils. *Soil Bull.* **2022**, *53*, 1220–1227.
3. Zeng, X.; Su, J.; Wang, H.; Gao, T. Centrifuge Modeling of Chloride Ions Completely Breakthrough Kaolin Clay Liner. *Sustainability* **2022**, *14*, 6976. [[CrossRef](#)]
4. Du, Y.-J.; Jin, F.; Liu, S.-Y.; Chen, L.; Zhang, F. Review of stabilization/solidification technique for remediation of heavy metals contaminated lands. *Yantu Lixue = Rock Soil Mech.* **2011**, *32*, 116–124.
5. Liu, S. Geotechnical investigation and remediation for industrial contaminated sites. *Chin. J. Geotech. Eng.* **2018**, *40*, 1–37.
6. Liu, Y.; Bouazza, A.; Gates, W.; Rowe, R. Hydraulic performance of geosynthetic clay liners to sulfuric acid solutions. *Geotext. Geomembr.* **2015**, *43*, 14–23. [[CrossRef](#)]
7. Zhang, Y.; Su, J.; Jiang, W.; Huang, Z.; Xiang, Y.; Zeng, F. Study on the Heavy Metal Pollution Evaluation and Countermeasures of Middle Size and Small Cities in Typical Drainage Area-Taking Xiangtan Reach of Xiangjiang River as an Example. *Res. J. Chem. Environ.* **2012**, *16*, 172–179.
8. Zhang, Y.; Xiang, Y.; Yu, G.; Yuan, K.; Wang, X.; Mo, H. Classification of environmental disaster in Hunan Province. *Disaster. Adv.* **2012**, *5*, 1756–1759.
9. Zhang, Y.; Huang, F. Indicative significance of the magnetic susceptibility of substrate sludge to heavy metal pollution of urban lakes. *ScienceAsia* **2021**, *47*, 374. [[CrossRef](#)]
10. Fetter, C.W.; Boving, T.; Kremer, D. *Contaminant Hydrogeology*; Waveland Press: Long Grove, IL, USA, 2017.
11. Zeng, X.; Li, Y.; Liu, X.; Yao, J.; Lin, Z. Relationship between the Shear Strength and the Depth of Cone Penetration in Fall Cone Tests. *Adv. Civ. Eng.* **2020**, *2020*, 8850430. [[CrossRef](#)]
12. Zeng, X.; Liu, X.; Li, Y.-H. The breakthrough time analyses of lead ions in CCL considering different adsorption isotherms. *Adv. Civ. Eng.* **2020**, *2020*, 8861866. [[CrossRef](#)]
13. Li, Y.; Zeng, X.; Lin, Z.; Su, J.; Gao, T.; Deng, R.; Liu, X. Experimental study on phosphate rock modified soil-bentonite as a cut-off wall material. *Water Supply* **2022**, *22*, 1676–1690. [[CrossRef](#)]
14. Gao, G.; Feng, S.; Ma, Y.; Zhan, H.; Huang, G. Kinetic model and semi-analytical solution for reactive solute transport considering dispersive scale effects and immobile water bodies. *Hydrodyn. Res. Prog. A Ser.* **2010**, *25*, 206–216.
15. Xie, H.; Tang, X.; Chen, Y. One-dimensional model for contaminant diffusion through layered media. *J.-Zhejiang Univ. Eng. Sci.* **2006**, *40*, 2191.
16. Selim, H. Transport of Reactive Solutes during Transient, Unsaturated Water Flow in Multilayered SOILS1. *Soil Sci.* **1978**, *126*, 127–135. [[CrossRef](#)]
17. Foote, G.J. Transit-time design for diffusion through composite liners. *J. Geotech. Geoenviron. Eng.* **2002**, *128*, 590–601. [[CrossRef](#)]
18. Chen, Y.-M.; Xie, H.-J.; Ke, H.; Tang, X.-W. Analytical solution of one-dimensional diffusion of volatile organic compounds (VOCs) through composite liners. *Yantu Gongcheng Xuebao* **2006**, *28*, 1076–1080.
19. Rowe, R.; Booker, J.R. The analysis of pollutant migration in a non-homogeneous soil. *Geotechnique* **1984**, *34*, 601–612. [[CrossRef](#)]
20. Yu, C.; Wang, H.; Fang, D.; Ma, J.; Cai, X.; Yu, X. Semi-analytical solution to one-dimensional advective-dispersive-reactive transport equation using homotopy analysis method. *J. Hydrol.* **2018**, *565*, 422–428. [[CrossRef](#)]
21. Zeng, X.; Wang, H.; Yao, J.; Li, Y. Analysis of Factors for Compacted Clay Liner Performance Considering Isothermal Adsorption. *Appl. Sci.* **2021**, *11*, 9735. [[CrossRef](#)]
22. Zhan, L.-T.; Zeng, X.; Li, Y.; Chen, Y. Analytical solution for one-dimensional diffusion of organic pollutants in a geomembrane-bentonite composite barrier and parametric analyses. *J. Environ. Eng.* **2014**, *140*, 57–68. [[CrossRef](#)]
23. Liu, X.; Chen, Y.; Zhang, W.; Chi, Y.; Guo, Z.; Xiao, J.; Hu, J. Effects of pH, ionic strength, time and temperature on the sorption of Cd (II) to illite. *J. Nucl. Radiochem.* **2012**, *34*, 358–363.
24. Zhang, J. Thermodynamic and Mechanistic Study on the Adsorption of Concave Barite Clay for the Treatment of Lead Containing Wastewater and Highly Fluorinated Water. Master's Thesis, Peking University, Beijing, China, 2008.
25. Rao, S.N.; Mathew, P.K. Effects of exchangeable cations on hydraulic conductivity of a marine clay. *Clays Clay Miner.* **1995**, *43*, 433–437. [[CrossRef](#)]
26. Zhu, W.; Xu, H.-Q.; Wang, S.-W.; Fan, X.-H. Influence of CaCl₂ solution on the permeability of different clay-based cutoff walls. *Rock Soil Mech.* **2016**, *37*, 1224–1230.
27. Malusis, M.A.; McKeehan, M.D. Chemical compatibility of model soil-bentonite backfill containing multiswellable bentonite. *J. Geotech. Geoenviron. Eng.* **2013**, *139*, 189–198. [[CrossRef](#)]
28. Bohnhoff, G.L.; Shackelford, C.D. Hydraulic conductivity of polymerized bentonite-amended backfills. *J. Geotech. Geoenviron. Eng.* **2014**, *140*, 04013028. [[CrossRef](#)]
29. Xu, H.; Shu, S.; Wang, S.; Zhou, A.; Jiang, P.; Zhu, W.; Fan, X.; Chen, L. Studies on the chemical compatibility of soil-bentonite cut-off walls for landfills. *J. Environ. Manag.* **2019**, *237*, 155–162. [[CrossRef](#)]
30. Pickens, J.F.; Grisak, G.E. Modeling of scale-dependent dispersion in hydrogeologic systems. *Water Resour. Res.* **1981**, *17*, 1701–1711. [[CrossRef](#)]

31. Singh, M.K.; Mahato, N.K.; Kumar, N. Pollutant's horizontal dispersion along and against sinusoidally varying velocity from a pulse type point source. *Acta. Geophys.* **2015**, *63*, 214–231. [[CrossRef](#)]
32. Barry, D.; Sposito, G. Analytical solution of a convection-dispersion model with time-dependent transport coefficients. *Water Resour. Res.* **1989**, *25*, 2407–2416. [[CrossRef](#)]
33. Zamani, K.; Bombardelli, F.A. Analytical solutions of nonlinear and variable-parameter transport equations for verification of numerical solvers. *Environ. Fluid Mech.* **2014**, *14*, 711–742. [[CrossRef](#)]
34. Guerrero, J.P.; Pontedeiro, E.; van Genuchten, M.T.; Skaggs, T. Analytical solutions of the one-dimensional advection–dispersion solute transport equation subject to time-dependent boundary conditions. *Chem. Eng. J.* **2013**, *221*, 487–491. [[CrossRef](#)]
35. Basha, H.; El-Habel, F. Analytical solution of the one-dimensional time-dependent transport equation. *Water Resour. Res.* **1993**, *29*, 3209–3214. [[CrossRef](#)]
36. Singh, M.K.; Ahmad, S.; Singh, V.P. Analytical solution for one-dimensional solute dispersion with time-dependent source concentration along uniform groundwater flow in a homogeneous porous formation. *J. Eng. Mech.* **2012**, *138*, 1045–1056. [[CrossRef](#)]
37. Yates, S. An analytical solution for one-dimensional transport in heterogeneous porous media. *Water Resour. Res.* **1990**, *26*, 2331–2338. [[CrossRef](#)]
38. Kumar, A.; Jaiswal, D.K.; Kumar, N. Analytical solutions to one-dimensional advection–diffusion equation with variable coefficients in semi-infinite media. *J. Hydrol.* **2010**, *380*, 330–337. [[CrossRef](#)]
39. Crank, J. *The Mathematics of Diffusion*; Oxford University Press: Oxford, UK, 1979.
40. Ogata, A.; Banks, R.B. *A Solution of the Differential Equation of Longitudinal Dispersion in Porous Media*; US Government Printing Office: Washington, DC, USA, 1961.
41. Li, Y.C.; Cleall, P.J. Analytical solutions for advective–dispersive solute transport in double-layered finite porous media. *Int. J. Numer. Anal. Methods Geomech.* **2011**, *35*, 438–460. [[CrossRef](#)]
42. Chen, Z.; Luo, B.; Wang, Z.; Huang, Z. Effect of temperature on the impermeability of landfill impermeable layers. *Environ. Eng.* **2015**, *33*, 133–136.
43. Dong, J.; Wang, C.-L.; Yin, Y.; Lou, Q.-Z.; Wang, X.-S.; Yang, Z. Influences of the freezing and thawing action on the performance of landfill liners. *J. Jilin Univ.* **2011**, *41*, 541–544.
44. Chi, Y. Study on the Modification of Albite and Its Adsorption of Heavy Metal Ions. Master's Thesis, Qinghai Normal University, Xining, China, 2013.
45. Huang, R. Study on the Adsorption Characteristics and Soil Remediation Efficacy of Modified Bumpy Clay for Heavy Metals. Master's Thesis, Guangdong University of Technology, Guangzhou, China, 2020.
46. Lei, H.; Shi, J.Y.; Wu, X. Prediction of landfill temperature considering biodegradation. *Henan Sci.* **2018**, *36*, 584–592.
47. Guo, T. Experimental Study on the Influence of Temperature on the Permeability of Anti-Seepage Walls of Sand-Attapulgitic Soil. Master's Thesis, Yangzhou University, Yangzhou, China, 2022.
48. Fan, R.; Du, Y.; Liu, S.; Yang, Y. Experimental study on the chemical compatibility of sand-bentonite vertical barrier materials under the action of inorganic salt solutions. *Geotechnics* **2020**, *41*, 736–746. [[CrossRef](#)]

Disclaimer/Publisher's Note: The statements, opinions and data contained in all publications are solely those of the individual author(s) and contributor(s) and not of MDPI and/or the editor(s). MDPI and/or the editor(s) disclaim responsibility for any injury to people or property resulting from any ideas, methods, instructions or products referred to in the content.